ACI STRUCTURAL JOURNAL TECHNICAL PAPER

Title no. 100-S9

Influence of Tension Strain on Buckling of Reinforcement in Concrete Columns

by Matthew J. Moyer and Mervyn J. Kowalsky

The research described in this paper presents a hypothesis regarding the influence of tension strain on buckling in reinforced concrete columns that is based primarily on the kinematics of member deformation. This is then followed by a presentation of a series of four large-scale column tests aimed at investigating the proposed mechanism. The test columns are of identical proportions and reinforcement content, with the only variable being the applied load history. Based on the results, it is apparent that the amount of tension strain that reinforcing bars within concrete columns are subjected to directly effects the buckling phenomena upon reversal of loading.

Keywords: buckling; column; strain.

BACKGROUND AND INTRODUCTION

Over the last 30 years, significant advances have been made in understanding the seismic behavior of concrete structures. Particular emphasis has been placed on developing details that aim to ensure ductile response in accordance with capacity design principles.[1] In the case of bridge columns, research has resulted in knowledge relating to lap-splice failures, shear failures, and confinement failures. As these undesirable modes of deformation have been addressed through proper detailing of transverse and longitudinal reinforcement, most well-designed modern bridge columns are likely to have their ultimate limit state governed by buckling of longitudinal reinforcement, as all other modes of failure are protected against.

At the same time that research on seismic behavior was underway, the concept of performance-based engineering, where structural systems are designed to achieve predefined levels of damage for discrete levels of seismic attack, gained favor. This is arguably not a new concept, as good engineers have sought to achieve such designs for many years. It is clear, however, that for performance-based engineering to be applied to its fullest potential, it is essential to have the ability to predict performance at various limit states ranging from the serviceability limit state to the survival limit state. As a result, it is felt to be essential to have an adequate understanding of the longitudinal bar buckling failure mode for the design of concrete bridge columns.

RESEARCH OBJECTIVE

The goals of this research are as follows: 1) re-evaluate the parameters that influence buckling of longitudinal reinforcement, focusing on the effects of tension strain, and hypothesize an alternative mechanism; 2) conduct experimental studies on large-scale bridge columns in an effort to investigate the hypothesis; and 3) apply the model in a format that would allow estimation of the column deformation at which buckling of reinforcement is likely to occur.

RESEARCH REVIEW

Extensive past research has been conducted in the area of buckling of longitudinal reinforcement. The majority of that research has focused on the monotonic behavior of reinforcing bars subjected to compression. There have also been some studies relating to the cyclic behavior of reinforcing bars, most notably work done by Rodriguez, Botero, and Villa[2] that concluded that reinforcing bars are most prone to buckling upon reversal from tension loading. In any case, the mechanism that is developed for reinforcing bars alone is quite different from that developed in reinforced concrete members, and only limited research has focused on this phenomena.

The connection between tension strain and the buckling phenomena in reinforced concrete members was first discussed by Paulay and Priestley[3] for structural walls. In their research, Paulay and Priestley postulated that the region of the wall subjected to high tension strains due to in-plane lateral load would be prone to buckle in the out-of-plane direction upon reversal of loading as the reinforcing bars become the sole source for compression zone stability until the cracks close under compression.

A relation was developed (Eq. (1)) between peak tensile strain ε_{sm}, length of buckled wall l_o, wall width b, reinforcement location factor β, and out-of-plane displacement factor ζ. A stability criterion was then developed to determine the maximum permissible out-of-plane displacement factor ζ as a function of the mechanical reinforcement ratio m, as shown in Eq. (2). Taken together, the maximum allowable tension strain in the in-plane direction can be determined for a given set of wall details, or vice-versa the required wall width b to sustain a prescribed tension strain ε_{sm} can be determined

$$\zeta = \frac{\varepsilon_{sm}}{8\beta}\left(\frac{l_o}{b}\right)^2 \tag{1}$$

$$\zeta \le \frac{1}{2}(1 + 2.35 - \sqrt{5.53m^2 + 4.70m}) \tag{2}$$

More recently, Chai and Elayer[4] proposed an alternative kinematic model for relating maximum tensile strain to out-of-plane displacement as shown in Eq. (3). The stability factor ζ in Eq. (3) is the same as that given by the work of Paulay and Priestley in Eq. (2); however, Eq. (3) clearly differs from

ACI Structural Journal, V. 100, No. 1, January-February 2003.
MS No. 01-409 received December 7, 2001, and reviewed under Institute publication policies. Pertinent discussion will be published in the November-December 2003 *ACI Structural Journal* if received by July 1, 2003.

Matthew J. Moyer *is a graduate research assistant in the Department of Civil Engineering at North Carolina State University, Raleigh, N.C.*

ACI member **Mervyn J. Kowalsky** *is an assistant professor in the Department of Civil Engineering at North Carolina State University, Raleigh, N.C. He is a member of ACI Committees 213, Lightweight Aggregate and Concrete; and 374, Performance-Based Seismic Design of Concrete Buildings; and Joint ACI-ASCE Committee 530, Masonry Standards.*

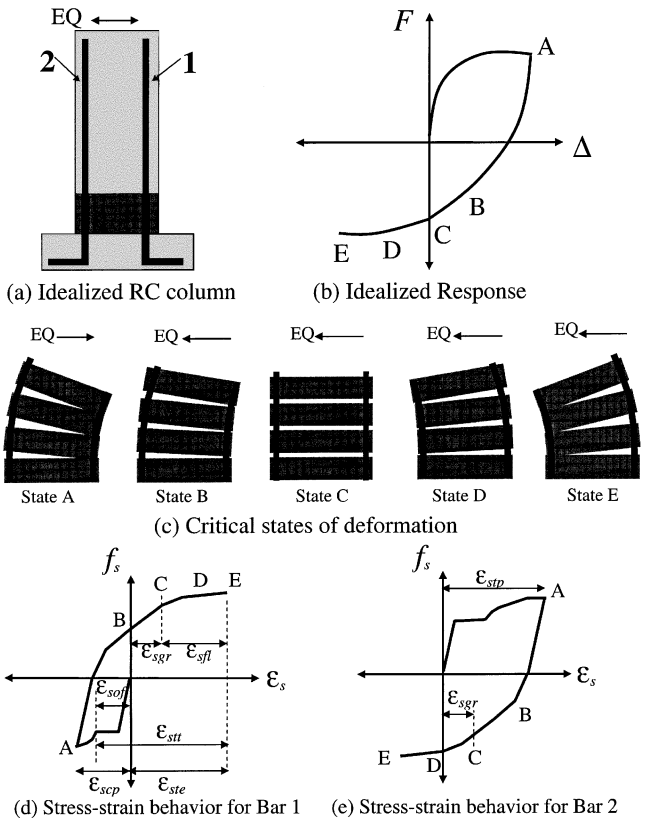

(a) Idealized RC column (b) Idealized Response

(c) Critical states of deformation

(d) Stress-strain behavior for Bar 1 (e) Stress-strain behavior for Bar 2

Fig. 1—Parameters of buckling mechanism.

Eq. (1). Chai and Elayer conducted experimental studies on square concrete columns subjected to reversed pure axial tension and compression. Their tests modeled the critical end regions of structural walls where out-of-plane buckling is likely to occur

$$\varepsilon_{sm} = \frac{\pi^2}{2}\left(\frac{b}{l_o}\right)\zeta + 3\varepsilon_y \quad (3)$$

Although the buckling mechanisms described by Paulay and Priestley[3] and Chai and Elayer[4] involve member buckling rather than reinforcement bar buckling, the basic concept that reinforcing bars represent the sole source for compression zone stability will be important in development of the model proposed in this paper.

DESCRIPTION OF TENSION-BASED BUCKLING MECHANISM

Preliminary definitions

Consider Fig. 1(a), which represents an idealized reinforced concrete column subjected to lateral loading. The bar numbered 1 represents the extreme compression bar upon loading to the right, while the bar numbered 2 represents the extreme tension bar upon the loading to the right.

Shown in Fig. 1(b) is an idealized force-displacement hysteretic response for one cycle of loading with five states identified as A, B, C, D, and E. A graphical display of the various states is shown in Fig. 1(c). As the column approaches State A as shown at the location marked A in the force-displacement envelope of Fig. 1(b), the stress state of Bars 1 and 2 are represented by the state marked A on the stress-strain curves of Fig. 1(d) and (e), respectively. From Fig. 1(d) and (e), the peak steel compression strain ε_{scp} and peak steel tension strain ε_{stp} are defined.

Upon reversal, the column passes through a state where the stress in Bar 1 is equal to zero. This point represents the new origin for the stress-strain curve for the steel, and the strain at this point is defined as the offset steel strain ε_{sof} (Fig. 1(d)). Upon further loading, the column passes through State B where cracks start to open on the Bar 1 side, as shown in Fig. 1(c). As the column displacement passes through zero at State C, the strain in Bar 2 has not yet returned to zero as shown in Fig. 1(e). Similarly, to ensure compatibility of deformation, the absolute strain in Bar 1 must be equal to the strain in Bar 2, and as such is greater than zero. This residual growth strain is referred to as ε_{sgr} as shown by State C in Fig. 1(d) and (e). As the column is loaded further, the cracks close on the Bar 2 side (State D in Fig. 1(c)), while the cracks on the Bar 1 side that opened at State B continue to widen. Upon further loading to State E, the stress-strain condition in the reinforcing bars is now characterized by State E in Fig. 1(d) and (e). Bar 1 at this point has been subjected to a total tension strain ε_{stt}, which is measured from the point of zero strain. The total steel tension strain ε_{stt} consists of three components: one due to the strain offset ε_{sof}, one due to growth ε_{sgr}, and one due to flexural deformation as measured from zero column displacement ε_{sfl}. The effective steel tension strain ε_{ste} is a critical parameter that represents the tension strain induced in the reinforcing bars starting from the point at which flexural cracks open (State B).

The last variable, ε_{scc}, represents the characteristic compression strain that a bar can sustain on its own before buckling occurs. This variable is largely a function of transverse steel ratio and the stress history that the reinforcing bars have been subjected to. For example, as the applied total tension strain ε_{stt} increases, the characteristic compression strain capacity decreases ε_{scc}.[2]

In summary, there are eight key strain variables in the proposed buckling model. They are: (1) peak steel compression strain ε_{scp}; 2) peak steel tension strain ε_{stp}; 3) residual steel growth strain at zero displacement ε_{sgr}; 4) flexural steel tension strain induced between zero displacement and maximum displacement ε_{sfl}; 5) offset steel tension strain defined as the strain at zero stress ε_{sof}; 6) total steel tension strain after reversal ε_{stt}; 7) effective steel tension strain after reversal ε_{ste}; and 8) characteristic steel compression strain capacity ε_{scc}. In the subsequent section, these eight strain variables are used to characterize a tension-based buckling model.

Model description

The basis of the proposed model relies on the recognition that reinforcing bars represent the sole source for compression zone stability in a fully cracked section. Consider the following scenario while again referring to Fig. 1. Upon reversal from State A, Bar 2, which was subjected to a peak tension strain of ε_{stp} (Fig. 1(e)), is subjected to compression stress as it unloads towards State B. Similarly, Bar 1, which was subjected to a peak compression strain of ε_{scp} (Fig. 1(d)), is placed in tension as it passes zero stress on the way to State B. Bar 2 must carry the entire compressive strain demand until the

cracks in the section at the Bar 2 location close (State D), at which time the concrete contributes to the compression zone stability and buckling is postponed. Therefore, the propensity for buckling in a reinforced concrete section will be tied directly to the maximum crack width, and hence the maximum tension strain that the critical section is subjected to. The maximum tension strain, by definition, represents the strain that the reinforcing bars must sustain upon reversal in compression that will result in crack closure and the commencement of contribution of the concrete to compression zone stability. For Bar 2, this is equal to the peak tensile strain ε_{stp} minus the yield strain ε_y. At the same time, the reinforcing bars have a characteristic compression strain capacity ε_{scc} that they can sustain depending on the confinement details, axial load ratio, longitudinal steel ratio, and stress-strain history. As long as the peak tensile strain minus the yield strain is less than the characteristic compression strain capacity ε_{scc}, buckling will not occur on the Bar 2 side.

Upon further loading, the critical side shifts to the Bar 1 side. Referring to Fig. 1(d), Bar 1 is now subjected to a total tension strain of ε_{stt} at State E on Fig. 1. This total tension strain consists of three components as shown in Fig. 1(d) and Eq. (4). The component due to the offset, ε_{sof}, represents the approximate origin shift due to the cyclic loading and can be approximated by Eq. (5). The component due to growth, ε_{sgr}, which manifests itself as an offset as shown in Fig. 1(d) and (e), will be a function of the steel constitutive relationship and the loading history. As inelastic cycles are accumulated, the growth strain increases. The component due to bending represents the tension strain obtained from flexural strength theory between the point of zero displacement (State C) and the point of maximum displacement (State E).

$$\varepsilon_{stt} = \varepsilon_{sof} + \varepsilon_{sgr} + \varepsilon_{sfl} \quad (4)$$

$$\varepsilon_{sof} = \varepsilon_{scp} - \varepsilon_y \quad (5)$$

The effective steel tension strain that represents the tension strain during which the concrete is cracked on the tension side is given by Eq. (6). To avoid buckling upon reversal from State E, Bar 1 must sustain in compression a strain equal to ε_{ste} in much the same way that Bar 2 was required to sustain a total strain in compression of ε_{stp} minus the yield strain during the previous cycle of loading. Even if the column is displaced to an equal amount in each direction, the effective tension strain on the Bar 1 side will be greater than that on the Bar 2 side due to column growth, which only occurs after reversal of loading. Similarly, if the member does not experience buckling after one cycle, continued cycling at the same displacement level will ultimately result in buckling as the growth strain ε_{sgr} accumulates. Ultimately, the effective steel tension strain demand on the extreme reinforcing bars ε_{ste} will exceed the characteristic compression strain capacity of the reinforcing bars ε_{scc}.

$$\varepsilon_{ste} = \varepsilon_{sgr} + \varepsilon_{sfl} \quad (6)$$

Significant features of proposed model

The proposed buckling mechanism contains four distinct features that are summarized as follows. First, buckling of reinforcement requires reversal of loading. If a column is subjected to a monotonic load, then buckling will not occur according to the model described in this paper. Under monotonic loading, reinforcing bars and surrounding concrete carry the compression load, and, as a result, stability of the reinforcing bars is assured. It is the expectation that for columns loaded in this manner, their failure would be governed by rupture of longitudinal reinforcement on the tension side of the column.

The second feature is that buckling of reinforcement requires significant tension strain to be developed in the reinforcing bars. This is a follow-up to the previous statement, and it is stated qualitatively. For reinforcing bars to buckle, they must be the sole source of compression zone stability for an amount of compressive deformation greater than they are able to sustain.

The third feature is related to the mechanism by which tension strain is accumulated in reinforcing bars in a reinforced concrete section. That is, tension strain is comprised of components due to strain offset, flexure, and growth. As a column is subjected to excursions in the inelastic range, the residual strain at zero displacement accumulates, and when added to the tension strain associated with the applied flexural deformation and the strain origin offset represents the total applied tension strain. To avoid buckling, the reinforcing bars must overcome in compression the components that occur while the section is cracked, namely, the flexural and growth components that, when taken together, result in the effective steel tension strain.

Lastly, buckling in the end occurs under compression, and existing models for prediction of compression strain capacity play an integral role in predicting the onset of buckling. Although the peak tension strain is identified as the key parameter that determines the stability of the reinforcing bars, it is only upon reversal when the reinforcing bars are placed into compression that buckling occurs. To develop a suitable model for prediction of maximum deformation capacity associated with buckling of reinforcement, it will be essential to evaluate existing models for prediction of compression capacity. The stability criterion developed by Paulay and Priestley[3] does not apply to this scenario as their model relates to local member buckling rather than buckling of reinforcing bars.

OVERVIEW OF EXPERIMENTAL PROGRAM

Purpose and overview of experimental program

The primary purpose of the experimental program is to investigate the hypothesis regarding the influence of tension strain on bar buckling as described in the previous section. To accomplish this, a series of four tests on large-scale reinforced concrete bridge columns were conducted with the only variable being the loading history.

The test specimens were circular reinforced concrete columns 18 in. (457 mm) in diameter with a cantilever height of 8 ft (2.44 m). Longitudinal reinforcement consisted of 12 No. 6 (19 mm diameter) Grade 60 (f_y = 414 MPa) reinforcing bars (longitudinal reinforcement ratio of 2.07%), while transverse reinforcement consisted of No. 3 (9.5 mm diameter) Grade 60 reinforcing spiral bars at 3 in. (76 mm) pitch (transverse volumetric steel ratio of 0.93%). Axial load in the amount of 52 k (231 kN) was applied to the test columns resulting in an axial load ratio of 5%. A drawing of the test specimen is shown in Fig. 2. Instrumentation consisted of strain gages applied to the longitudinal steel from levels 4 in. (102 mm) below the footing interface to 24 in. (610 mm) above the footing interface. Using the footing as a reference point, gages were placed at –4, 0, 4, 8, 16, and 24 in. (–102, 0, 102, 204, 408, and 610 mm) on the two extreme reinforcing bars. Gages were also placed on the transverse steel located at

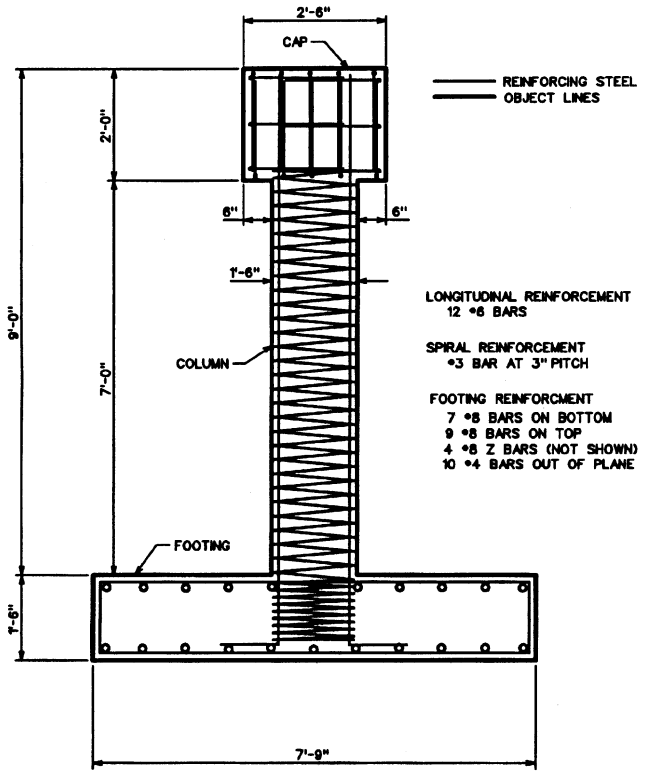

Fig. 2—Typical test specimen.

levels of 6, 12, 18, and 24 in. (152, 304, 456, and 610 mm) above the footing. At each level, two gages were placed on the column faces experiencing the highest confinement strains (north and south faces, which represent the direction of loading). External instrumentation consisted of linear potentiometers over the first 32 in. (813 mm) of the columns for measurement of column growth and section curvature. The lower 32 in. (813 mm) of the column were divided into four regions 8 in. (203 mm) in length. A string potentiometer was utilized to measure column top deformation. Load cells for measurement of axial load and applied lateral load were also utilized. A sketch of instrumentation locations is shown in Fig. 3. The test units were rigidly connected to the laboratory strong floor through the use of four 1-3/8 in. (35 mm) Dywidag bars. Figure 4 represents a photo of the test setup.

Loading histories for Units 1 and 2

As previously mentioned, the only variable in the four tests was the loading history. Before conducting the first test, the loading histories for Tests 1 and 2 were selected, with the first test identified as the control specimen. The loading history for Test 1 consisted of reversed single cycles to increments of 25, 50, 75, and 100% of the first yield force $F\text{¢}_y$ followed by subsequent three-cycle sets in displacement control to predefined increments of the equivalent yield displacement Δ_y. The equivalent yield displacement Δ_y for these calculations is obtained by extrapolating the experimentally measured displacement $\Delta\text{¢}_y$ at the analytical first yield force $F\text{¢}_y$ to the analytical ideal force capacity F_i, as in Eq. (7). The loading history for Unit 1 is shown graphically in Fig. 5(a) and (b).

$$\Delta_y = \frac{F_i}{F'_y}\Delta'_y \quad (7)$$

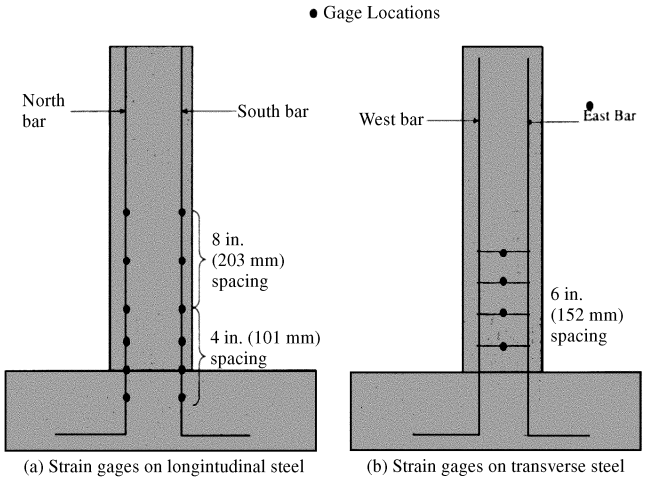

Fig. 3—Instrumentation.

For test Unit 2, the force control portion of the loading history was the same as Unit 1 (Fig. 5(a)). Beyond the yield point, the loading history was such that in one direction, it followed the same pattern as was applied to test Unit 1. Meanwhile, in the opposing direction, loading was applied only to the first yield displacement $\Delta\text{¢}_y$. A figure illustrating the loading history for test Unit 2 is shown in Fig. 5(c). The purpose of this loading history is to investigate the fundamental hypothesis of the proposed mechanism. By subjecting Unit 2 to lower levels of tension strain in one direction, it was expected that the displacement to induce buckling in the opposing direction would be significantly greater than that for test Unit 1. The following section describes the results of these first two tests.

TEST RESULTS FOR UNITS 1 AND 2

Unit 1 observations

Following the applied load history of Fig. 5, test Unit 1 sustained buckling of reinforcement after the third cycle at displacement ductility 4. For this, and all subsequent tests, buckling was first identified visually during the loading, and then confirmed by inspection of the force-deformation response, which typically indicates a reduction in lateral force capacity. The displacements reported reflect the maximum displacement achieved for the loading cycle prior to buckling. For test Unit 1, the column displacement was 5.9 in. (150 mm), resulting in a drift ratio of 6.1%. Figure 6 represents photos of the plastic hinge region at the ductility level that initiated buckling of reinforcement. The force-displacement hysteretic response is shown in Fig. 7, where the X marks approximately where buckling was first noted during the response. Note that, as expected, the column behaved in a dependable, flexural manner up to the failure level.

Figure 8 represents the readings of the linear potentiometer located in the first 8 in. (203 mm) of the column. Note the accumulation of permanent deformation (growth strain) with increasing cycles of deformation. Figure 9 represents a plot of the growth strain as a function of displacement ductility, with the peak growth strain from this plot nearly 2%. To determine the total steel tension strain the bars were subjected to before the initiation of buckling, the flexural tension strain is estimated analytically from the applied deformation of 5.9 in. (150 mm). For this level of deformation, a value of 4.5% is estimated (note that it was not possible to evaluate the experimental tension strains due to flexure as the

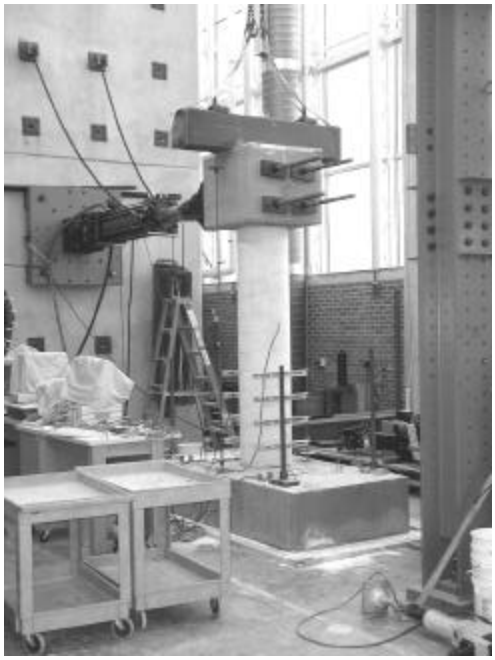

Fig. 4—Test setup.

strain gages applied to the reinforcing bars ceased operation at a much lower level of tension strain). The flexural tension strain is then added to the experimentally measured growth strain of 2% to determine the total steel tension strain.

Unit 2 observations

Following the applied load history of Fig. 5(a) and (c), test Unit 2 first exhibited buckling upon the first return cycle from a displacement ductility level of 7. The maximum applied displacement was 10.3 in. (262 mm) (10.7% drift ratio). Figure 10 represents a photo of the plastic hinge region at buckling, while Fig. 11 represents the force-displacement hysteretic response. For this test unit, buckling of reinforcing bars occurred on the side of the column that was subjected to high level of tension strains (north side) and low levels of compression strains. On the opposing side (south side) of the column that was subjected only to tensile yield strain, buckling was permanently postponed, thus, supporting the hypothesis that the level of tension strain induced in reinforcing bars correlates directly with propensity for buckling.

TEST UNIT 3

Loading history

In selecting the loading history for test Unit 3, the results of test Unit 2 were consulted. It was clear from the behavior of Unit 2 that by subjecting the test column to low levels of tension strain, buckling was postponed. It was also clear from the opposing side of the column that under large tensile strains, buckling occurred under relatively small levels of compression. In this test, the objective was to determine the significance of cyclic loading and the accumulation of growth strain that accompanies it. The loading history, which is shown in Fig. 12, consists of a single cycle to a displacement ductility of 7, which represents the maximum displacement that test column two was able to sustain before buckling on reversal. Loading was paused during testing at each ductility increment for test observation. If cyclic loading and the corresponding growth strain are not critical, then it is

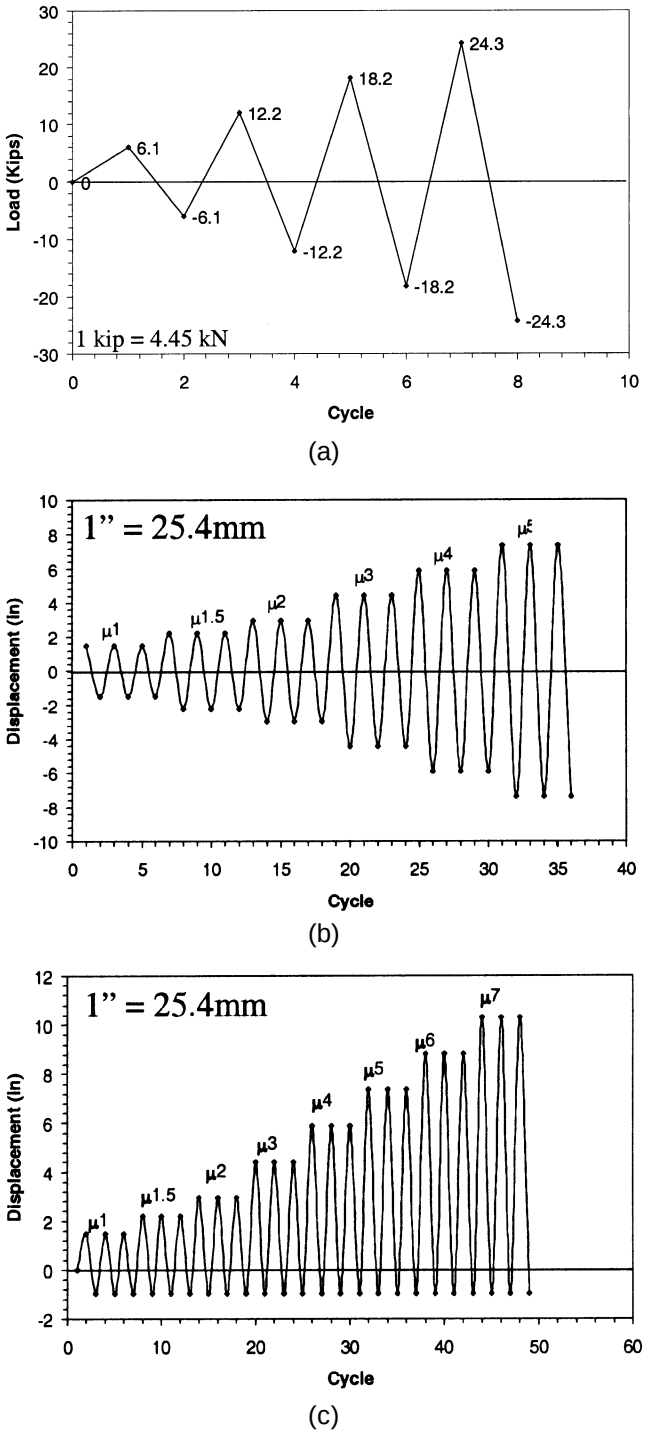

Fig. 5—Load history for Units 1 and 2: (a) force control loading for Units 1 and 2; (b) displacement control loading for Unit 1; and (c) displacement control loading for Unit 2.

expected that the reinforcing bars would buckle upon reversal from displacement ductility of 7.

Test observations

Figure 13 contains a photo of the test Unit 3 illustrating the buckling of the reinforcing bars, while Fig. 14 represents the force-displacement hysteretic response for test Unit 3. It is noted that unlike test Specimen 2, buckling did not occur upon reversal from a displacement ductility of 7. The column was able to sustain a deformation of equal amount in the opposing direction without any signs of buckling. It was

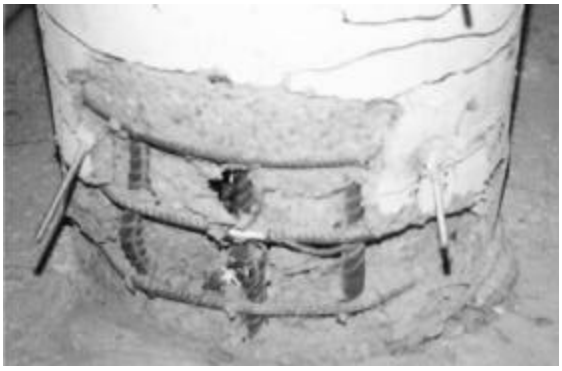

Fig. 6—Buckling of reinforcement in test Unit 1.

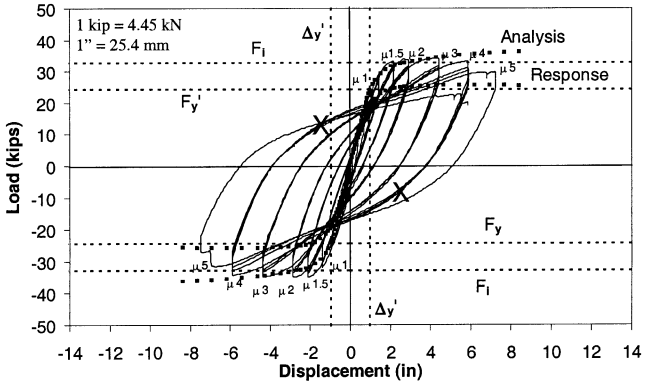

Fig. 7—Force-displacement hysteretic response for Unit 1.

only upon reversal from the return cycle that buckling initiated. This test therefore confirmed that the tensile strain accumulated due to cycling must be considered in conjunction with the flexural tension strain.

TEST UNIT 4

Loading history

The loading history for Unit 4 (Fig. 15) was similar to Unit 3, except that the final displacement ductility level was increased from 7 to 9. By applying a deformation consistent with a displacement ductility of 9, the tension strain in the extreme reinforcing bar due to flexure alone exceeds the combined flexure and growth from the previous test specimen. As a result, if the hypothesis is correct, it would be expected that the reinforcing bars would buckle upon reversal from a displacement ductility of 9 without any further cycling.

Test observations

Figure 16 represents the force-displacement hysteretic response for Unit 4. As expected, buckling of reinforcement, which is shown in Fig. 17, occurred upon reversal from a displacement ductility of 9 prior to the point at which the cracks closed. This test illustrated that the most important parameter is total tensile strain, and that the strain may be accumulated due to growth and flexure as in Tests 1, 2, and 3, or due to flexure alone as in Test 4.

SUMMARY OF EXPERIMENTAL PROGRAM

A series of four tests were conducted with their results summarized in Table 1. The interested reader is referred to reference 5 for more details. Based on the experimental results, the following observations are offered:

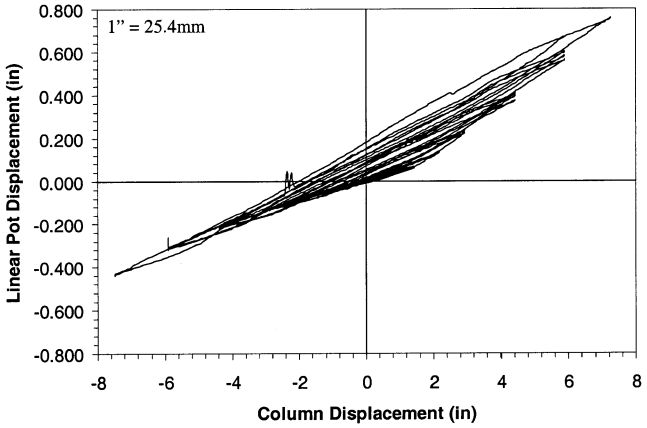

(a) north side

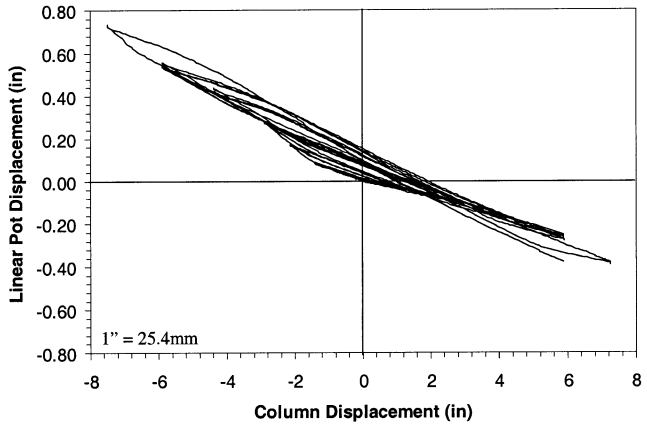

(b) south side

Fig. 8—Unit 1 measured column growth over first 8 in. of column.

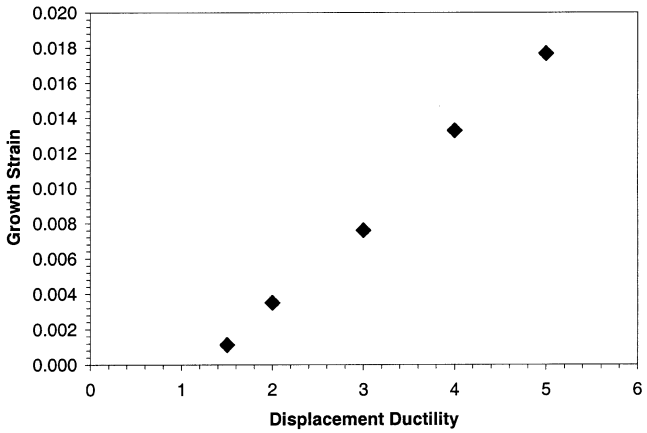

Fig. 9—Growth strain versus displacement ductility for Unit 1.

1. The hypothesis that buckling of reinforcing bars is directly related to the peak tensile strain applied seems to have been confirmed. The mechanism recognizes that reinforcing bars placed in tension represent the sole source for compression zone stability upon reversal due to cracks in the concrete on the tension side. Until the cracks close in compression, the reinforcing bars are vulnerable to buckling; and

2. The peak tensile strain that may be sustained prior to buckling upon reversal can be accumulated through extensive cycling at low levels of response, or from only one cycle at very high levels of response. As a result, predicting the onset of

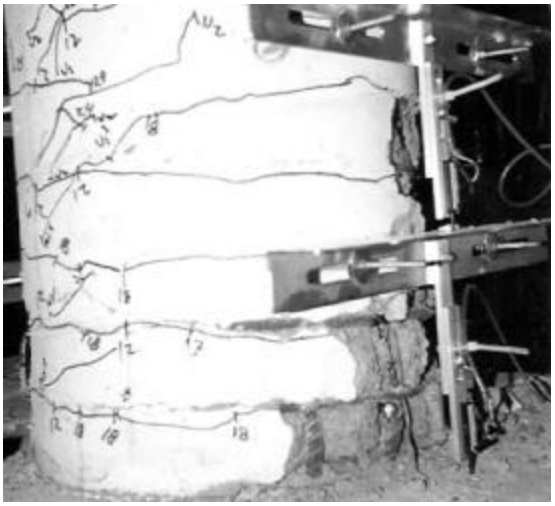

Fig. 10—Buckling of reinforcement for test Unit 2.

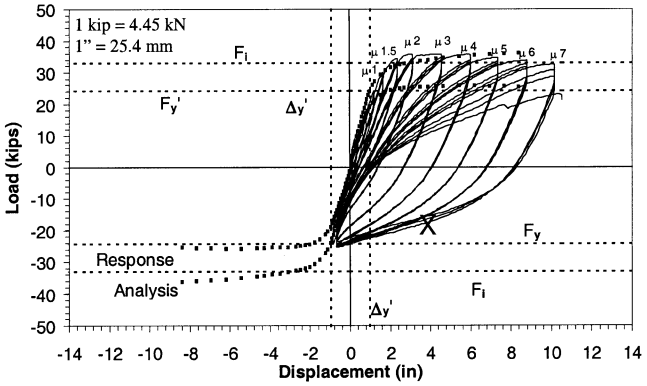

Fig. 11—Force-displacement hysteretic response for Unit 2.

buckling for a particular column will require some knowledge of the expected response history.

ASSESSMENT OF REINFORCEMENT BUCKLING LIMIT STATE

The model described previously in this paper was presented by considering one complete cycle of loading to a fixed deformation in the inelastic range. This, of course, does not represent a typical earthquake loading history. Many of the variables of the model will be largely a function of the applied load history, particularly the offset steel strain ε_{sof} and the growth strain ε_{sgr}. In turn, the growth strain will directly impact the effective steel tension strain ε_{ste}. To formulate expressions for prediction of bar buckling, it will be essential to develop models for prediction of these variables. Discussed in this section is a graphical application of the proposed mechanism, as well as some preliminary models for the variables that comprise the mechanism. It is important to note that preliminary models for the key variables in the mechanism may be updated or changed without affecting the basic premise behind the model.

Basic expression for proposed mechanism

The variable that is ultimately of interest from a design perspective is the flexural tension strain as measured from the point of zero column displacement ε_{sfl}. Once the allowable ε_{sfl} is obtained for a specific load history and column configuration, the allowable lateral deformation can be readily evaluated using the plastic hinge method for member

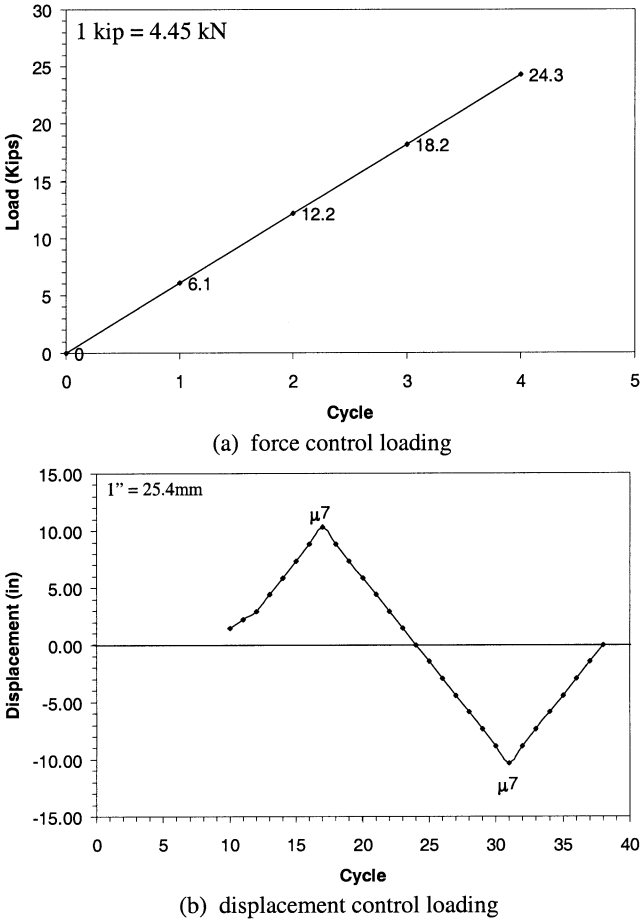

Fig. 12—Load history for Unit 3.

Fig. 13—Buckling of reinforcement in Unit 3.

deformation. As such, ε_{sfl} can be thought of as the tension strain limit to avoid buckling of longitudinal reinforcement. Referring to Fig. 1(d), Eq. (8) represents the expression for ε_{sfl}. The criteria for buckling can be expressed as Eq. (9). Substituting Eq. (9) into Eq. (8) results in Eq. (10)

$$\varepsilon_{sfl} = \varepsilon_{ste} - \varepsilon_{sgr} \quad (8)$$

$$\varepsilon_{ste} = \varepsilon_{scc} \quad (9)$$

$$\varepsilon_{sfl} = \varepsilon_{scc} - \varepsilon_{sgr} \quad (10)$$

Growth strain at zero displacement (ε_{sgr})

It is expected that the column growth strain is directly related to the peak tensile strain demand placed on the reinforcement

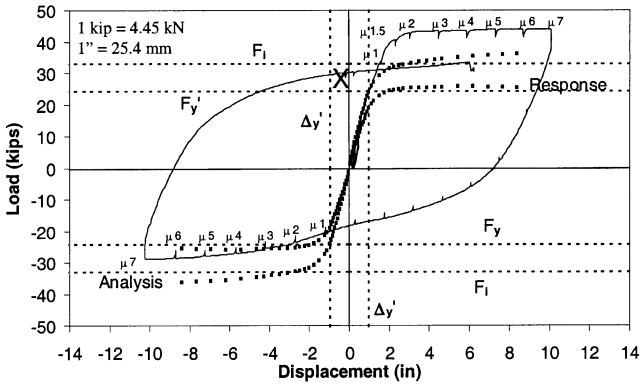

Fig. 14—Force-displacement hysteretic response for Unit 3.

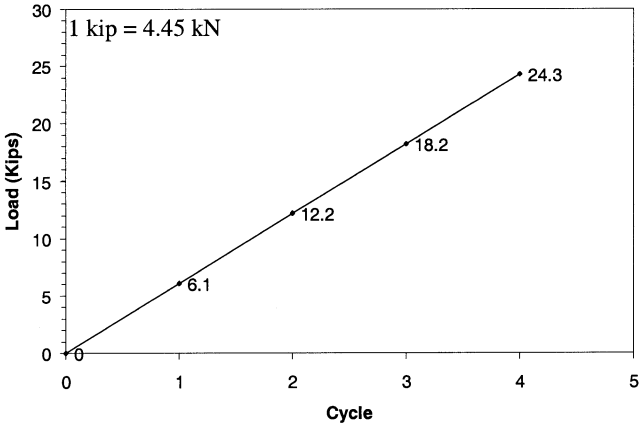

(a) force control loading

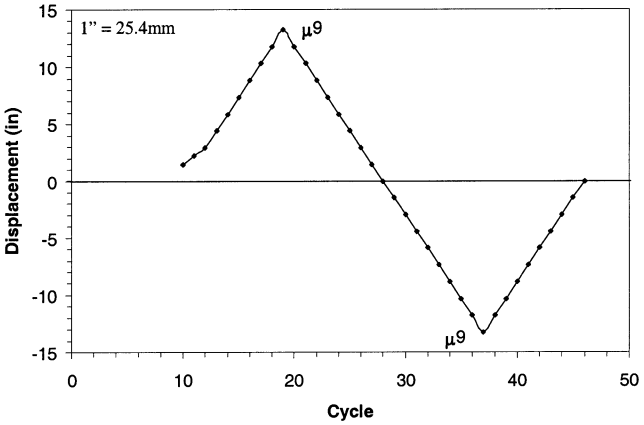

(b) displacement control loading

Fig. 15—Load history for Unit 4.

in the column. As the peak strain increases, the growth strain increases in proportion. To develop a suitable model for prediction of growth strain, two aspects must be considered: 1) the proportionality between peak and residual strain; and 2) the dependence of peak strain on axial load ratio, longitudinal steel ratio, and curvature ductility ratio.

Considering the second point first, using the parametric studies conducted by Kowalsky,[6] figures depicting the relationship between curvature ductility (defined as the inelastic curvature divided by the yield curvature), peak steel tension strain, axial load ratio, and longitudinal steel ratio can be developed as shown in Fig. 18. These charts, which were developed from a suite of moment curvature analysis on circular column sections, can then be used to determine the peak tension strain as a function of curvature ductility for

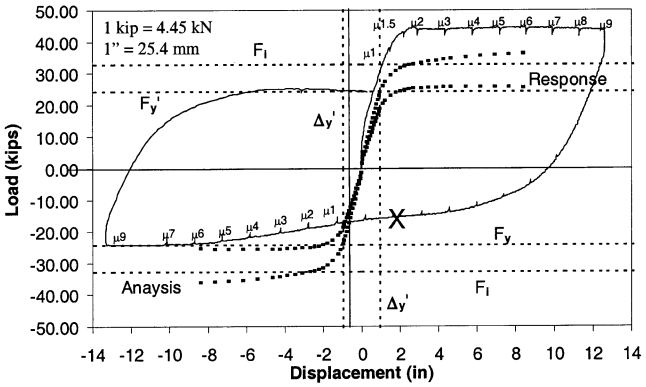

Fig. 16—Force-displacement hysteretic response for Unit 4.

Fig. 17—Buckling of reinforcement in Unit 4.

Table 1—Summary of experimental results

Test unit	Load history	Maximum displacement prior to buckling
One	Full cyclic in both directions.	5.9 in. (150 mm) (μ_Δ = 4)
Two	Full cyclic in one direction. Cyclic to yield in other direction.	10.3 in. (262 mm) (μ_Δ = 7)
Three	Cyclic at a constant displacement of 10.29 in. (262 mm)	10.3 in. (262 mm) (μ_Δ = 7) Two half-cycles at this level prior to buckling.
Four	Cyclic at a constant displacement of 13.23 in. (336 mm)	13.23 in. (336 mm) (μ_Δ = 9) Two half-cycles at this level prior to buckling.

a specific axial load ratio and longitudinal steel ratio. Instead of using the graphs in Fig. 18, Eq. (11), which attempts to capture the trends shown in Fig. 18, can be used. Note that Eq. (11) should only be used for axial load ratios between 0 and 0.4 and longitudinal steel ratios between 0.5 and 4%. The steel ratio ρ in Eq. (11) must be expressed as a percent, while the axial load ratio *ALR* is defined in Eq. (12)

$$\varepsilon_s = \frac{\mu_\phi}{(260 + 325ALR) + (20 - 25ALR)(\rho - 0.5)} \quad (11)$$

$$ALR = \frac{P}{f'_c A_g} \quad (12)$$

Estimation of the relationship between peak steel tension strain and growth strain can be accomplished by referring to the experimental results of the previous section. Figure 19 represented the growth strain as a function of column ductility for Tests 1 and 2. Beyond a curvature ductility of 4, the growth strain was determined to be approximately 50% of the peak

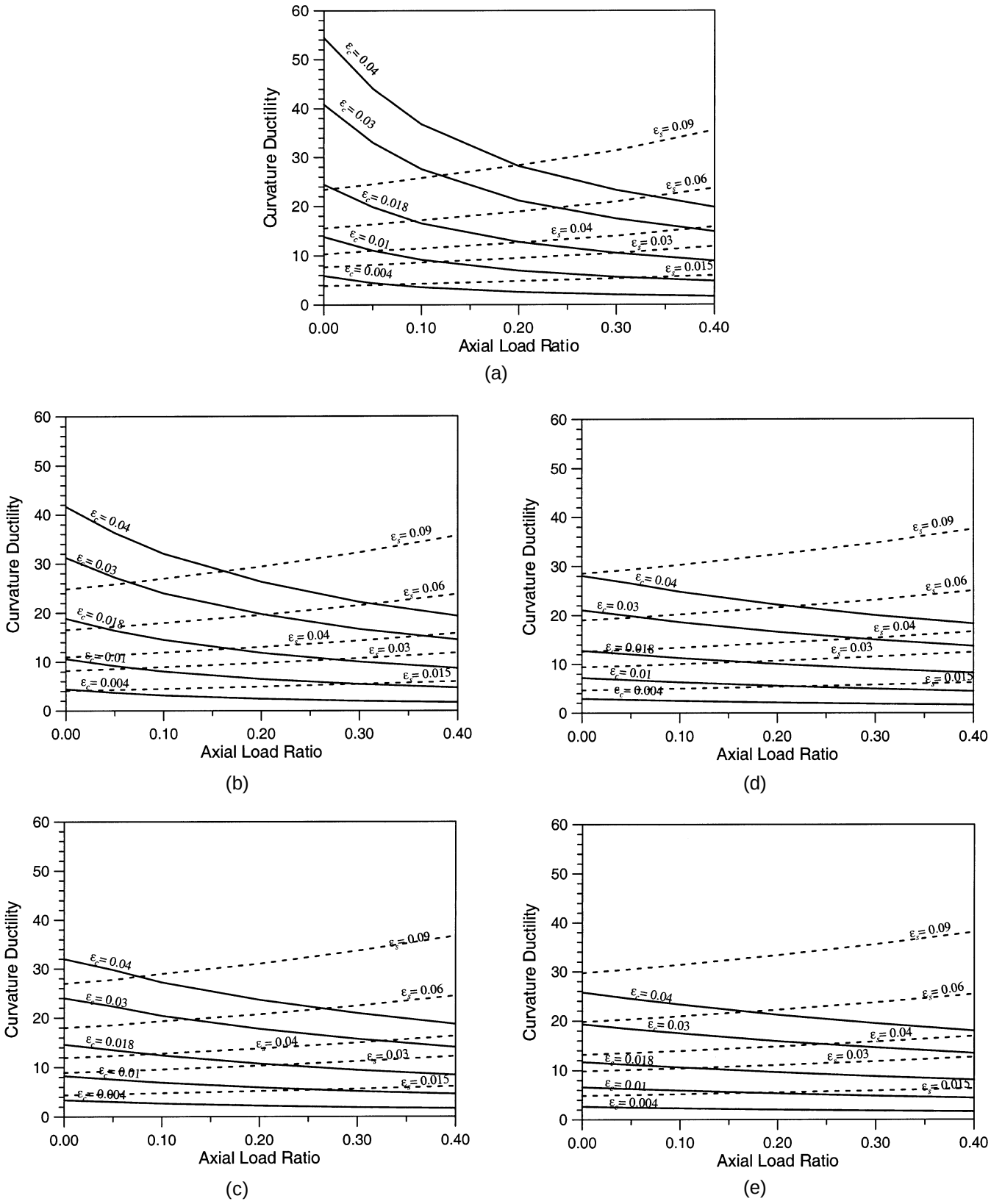

Fig. 18—Longitudinal steel ratio of (a) 0.5%; (b) 1%; (c) 2%; (d) 3%; and (e) 4%.

steel tension strain. It is clear that validation of this trend should be accomplished using a combination of experimental studies and cyclic section analysis; however, for the purposes of this paper, it is proposed that the growth strain be evaluated with Eq. (13) for curvature ductility factors equal to or greater than 4. Linear interpolation is proposed for evaluation of the growth strain between a curvature ductility of 1 (where the growth strain is zero), and 4 where it is given by Eq. (13). Further studies in the future may, of course, result in a different relationship than that shown in Eq. (13)

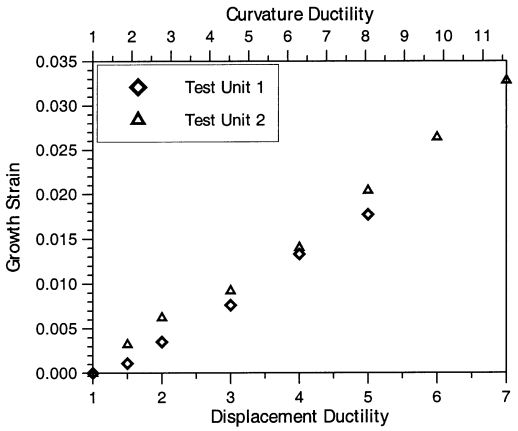

Fig. 19—Growth strain versus ductility for tests one and two.

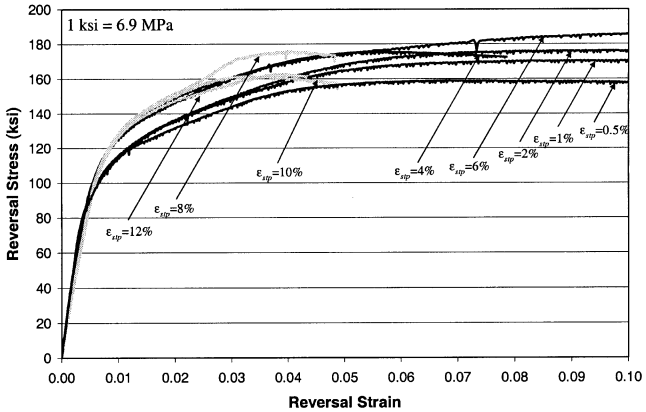

Fig. 20—Origin shifted stress-strain reversal curves.

$$\varepsilon_{sgr} = \frac{1}{2}\frac{\mu_\phi}{(260 + 325ALR) + (20 - 25ALR)(\rho - 0.5)} \quad (13)$$

Characteristic compression strain capacity (ε_{scc})

There are several existing models for assessment of compression strain capacity for reinforcing that are based on a variety of approaches ranging from empirical formulations to classical buckling approaches to nonlinear finite element analysis. A thorough review of these models can be found in Hose.[7] For this paper, a simple approach based on a modification of the secant-stiffness double modulus approach is used. It is noted that other models for compression strain capacity can be used if desired.

The basis of the double modulus approach is a reduction in elastic stiffness of reinforcing bars that is then incorporated into the traditional Euler buckling expression.[8] The reduction in elastic stiffness has been accomplished in the past by use of either the tangent[9] or secant modulus.[10] The double modulus expression is shown in Eq. (14) where E_i represents the initial modulus, and E_s represents the secant modulus. Note that E_s can be replaced with E_t when using the tangent modulus. The double modulus can then be evaluated as a function of strain, and the required spacing of transverse steel obtained with Eq. (15)[11] where s is the transverse steel spacing, d_{bl} is the longitudinal bar diameter, k is the effective length factor, and f_{max} the steel stress.

$$E_d = \frac{4E_sE_i}{(\sqrt{E_s} + \sqrt{E_i})^2} \quad (14)$$

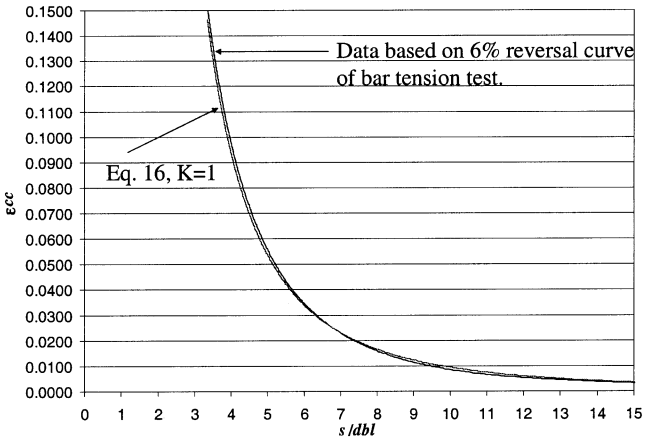

Fig. 21—Compression strain capacity versus s/d_{bl}.

$$\frac{s}{d_{bl}} = \frac{\pi}{4K}\sqrt{\frac{E_d}{f_{max}}} \quad (15)$$

For this paper, these calculations were obtained by using an experimental stress-strain reversal curve from a reinforcing bar initially subjected to a tension strain of 6%. Previous research by Hose[7] has shown that the stress versus strain reversal curve is not influenced significantly by the level of tension strain induced in the reinforcing bars. To verify this, a series of tests on reinforcing bars were conducted where eight equivalent specimens were subjected to tension strains of 0.5, 1, 2, 4, 6, 8, 10, and 12% prior to reversal. A clear length of 3 in. (76 mm) was used between the heads of the 220 kip (979 kN) MTS universal testing machine. The reversal curves were then plotted together where the origin of all curves is taken as the maximum tension strain prior to reversal. The results are shown in Fig. 20 where little difference is noted in compression behavior.

Using the 6% reversal curve from Fig. 20 for the calculations, Eq. (14) and (15) were evaluated at reversal strains ranging from 0.003 to 0.15 with the results shown as Fig. 21. Equation (16) represents a power best-fit equation to the data of Fig. 21 (assuming a value of $K = 1$) and allows evaluation of the characteristic compression strain capacity as a function of longitudinal bar diameter, transverse steel spacing, and effective length. As noted previously, Eq. (16) represents a suggested expression. Other expressions may be used within the mechanism described in this paper. Furthermore, the value of K will ultimately depend on whether reinforcing bars buckle between layers of transverse reinforcement or over several layers of transverse reinforcement. A study is currently underway by the second author that aims to evaluate the parameter K as a function of column details by analyzing the existing database of cyclic experimental test results on circular reinforced concrete bridge columns

$$\varepsilon_{cc} = 3\left(\frac{Ks}{d_{bl}}\right)^{-2.5} \quad (16)$$

Graphical representation for allowable flexural tension strain (ε_{sfl})

Given that the growth strain ε_{sgr} is a function of curvature ductility and that the flexural tension strain ε_{sfl} is also a function of curvature ductility, plotting both of these variables along with the characteristic compression strain capacity allows for

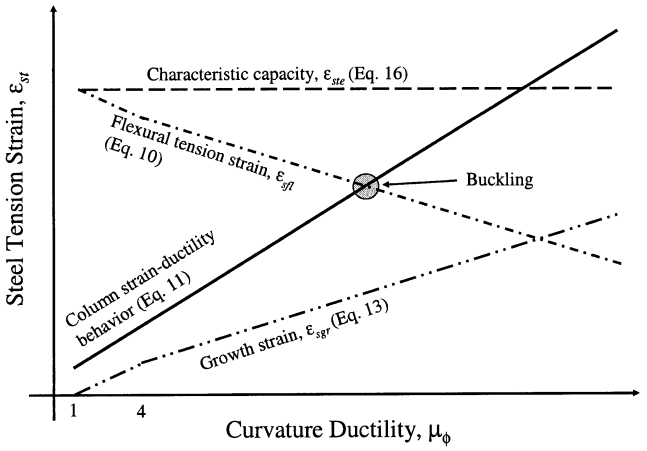

Fig. 22—Obtaining curvature ductility at reinforcing bar buckling.

a direct solution for the tension strain and hence curvature ductility to initiate buckling of the longitudinal reinforcement.

Consider Fig. 22, which represents a plot of tension strain ε_{st} versus curvature ductility μ_ϕ. The steps to construct such a graph for a column of given geometry are as follows:

1. Plot a line to represent the allowable effective tension strain ε_{ste}. From Eq. (9), $\varepsilon_{ste} = \varepsilon_{scc}$. A proposed expression for ε_{scc} was presented in the previous section (Eq. (16));
2. Plot a line to represent the growth strain ε_{sgr} as a function of μ_ϕ. A relationship for this expression was shown in Eq. (13);
3. Following Eq. (10), plot the allowable flexural tension strain ε_{sfl} as a function of μ_ϕ;
4. Plot a curve representing the tension strain versus curvature ductility behavior of the cross section. Eq. (11) provides such an expression; and
5. Determine the design flexural tension strain and corresponding curvature ductility by intersecting the line from Step 4 with the ε_{sfl} line from Step 3.

Alternatively, the calculation can be solved for numerically by setting Eq. (10) equal to Eq. (11) and solving for the curvature ductility factor μ_ϕ. The resulting expression is shown as Eq. (17) and represents the curvature ductility factor at the onset of buckling. Given the column axial load ratio, longitudinal steel ratio, spacing of transverse steel, effective length factor, and longitudinal bar diameter, the curvature ductility factor at the onset of buckling is then readily obtained.

$$\mu_\phi = 2\left(\frac{K s}{d_{bl}}\right)^{-2.5} Z \quad (17)$$

$$Z = ([260 + 325ALR] + [20 - 25ALR][\rho - 0.5]) \quad (18)$$

CONCLUSIONS AND FURTHER STUDIES

Presented in this paper was a hypothesis regarding the influence of tension strain on buckling in reinforced concrete columns that is based primarily on the kinematics of member deformation. Through a series of large-scale tests on reinforced concrete bridge columns, it was shown that the propensity for buckling of reinforcement under compressive stress is directly tied to the level of tensile strain the bars are initially subjected to. A model was proposed that can be used to determine the maximum tensile strain due to flexural deformation a reinforcing bar can be subjected to prior to initiation of buckling upon reversal of loading. Column displacement prior to initiation of buckling can then be obtained through the use of the plastic hinge method for member deformation. Future studies should focus largely on two aspects: 1) further evaluation of the growth strain ε_{sgr} as a function curvature ductility for a variety of column details; and 2) further evaluation of the characteristic compression strain ε_{scc} as a function of column details.

The growth strain will be difficult to evaluate experimentally from the existing database of test results due to the lack of availability of reliable strain gage data. As a result, the emphasis should be placed on an analytical study using fiber models where a variety of reinforced concrete column configurations could be analyzed under cyclic loads and the level of growth strain identified. Alternatively, this may also be accomplished through the use of cyclic moment curvature analysis.

The characteristic compression strain model used in this paper is left as a function of the effective length factor *K*, as shown in Eq. (17). The value of *K* will depend on whether longitudinal reinforcing bars buckle between layers of transverse steel or across several layers of transverse steel. An evaluation is currently underway that aims to assess the value of *K* from the large database of existing tests on circular reinforced concrete bridge columns.

ACKNOWLEDGMENTS

The research described in this paper was jointly supported by a North Carolina State University Faculty Research and Professional Development Grant and the Department of Civil Engineering. In addition, support in the form of materials donations was provided by AmeriSteel of Raleigh and Steel Specialties of Mississippi. Undergraduate student support was received from the NC State HHMI-Rise program and the NC State/National Taiwan University Exchange program that supported the contributions of Nathaniel Horner and Eddy Cheng. The authors would also like to thank Bryan Ewing for conducting material tests on reinforcing bars. The comments received during the review process were very helpful in ensuring a clear presentation of the research results, and the authors thank the reviewers for their diligent reading of the manuscript. Lastly, the authors would like to thank the technical staff of the NC State Constructed Facilities Laboratory, especially the efforts of Jerry Atkinson and Bill Dunleavy without whom this work would not have been possible.

REFERENCES

1. Paulay, T., and Priestley, M. J. N., *Seismic Design of Reinforced Concrete and Masonry Buildings*, Wiley-Interscience, N.Y., 1992.

2. Rodriguez, M. E.; Botero, J. C.; and Villa, J. "Cyclic Stress-Strain Behavior of Reinforcing Steel Including Effect of Buckling," *Journal of Structural Engineering*, ASCE, V. 125, No. 6, 1999, pp. 605-612.

3. Paulay, T., and Priestley, M. J. N., "Stability of Ductile Structural Walls," *ACI Structural Journal*, V. 90, No. 4, July-Aug. 1993, pp. 385-392.

4. Chai, Y. H., and Elayer, D. T., "Lateral Stability of Reinforced Concrete Columns under Axial Reversed Cyclic Tension and Compression," *ACI Structural Journal*, V. 96, No. 5, Sept.-Oct. 1999, pp. 780-789.

5. Moyer, M. J., and Kowalsky, M. J., "Influence of Tension Strain on Buckling of Reinforcement in RC Bridge Columns," *Structural Engineering and Mechanics Research Report* SEMR-2001/1, North Carolina State University, Raleigh, N.C., 2001.

6. Kowalsky, M. J., "Deformation Limit States and Implications on Design of Circular RC Bridge Columns," *Journal of Structural Engineering*, ASCE, V. 126, No. 8, 2000, pp. 869-878.

7. Hose, Y. H., "Seismic Performance and Failure Behavior of Plastic Hinge Regions in Flexural Bridge Columns," PhD thesis, Department of Structural Engineering, University of California, San Diego, Calif., 2001.

8. Euler, L., "Methodus Inveniendi Lineas Curvas Maximi Minimive Proprietate Gaudentes," Appendix I, "De Curvis Elasticis," Bousquet, Lausanne, and Geneva, 1744.

9. Gere, J. M., *Mechanics of Materials*, 5th Edition, Brooks/Cole, Pacific Grove, Calif., 2001.

10. Mander, J. B.; Priestley, M. J. N.; and Park, R., "Seismic Design of Bridge Piers," *Research Report* 84-2, University of Canterbury, Christchurch, New Zealand, 1984.

11. Kowalsky, M. J.; Priestley, M. J. N.; and Seible, F., "Flexural Behavior of Lightweight Concrete Bridge Columns Under Seismic Conditions," *Structural Systems Research Report* 96/08, Department of Structural Engineering, University of California, San Diego, Calif., 1996.